Catalysis Today 165 (2011) 145–149

Contents lists available at ScienceDirect

Catalysis Today

journal homepage: www.elsevier.com/locate/cattod

Water splitting on TiO_2 nanotube arrays

Qiang-qiang Meng[a,b], Jian-guo Wang[a,b,*], Qin Xie[a,b], Hua-qing Dong[a,b], Xiao-nian Li[a,b]

[a] State Key Laboratory Breeding Base of Green Chemistry Synthesis Technology, Hangzhou 310032, PR China
[b] Institute of Industrial Catalysis, College of Chemical Engineering and Materials Science, Hangzhou 310032, PR China

ARTICLE INFO

Article history:
Received 12 September 2010
Received in revised form
27 November 2010
Accepted 29 November 2010
Available online 12 January 2011

Keywords:
Density functional theory
Water splitting
TiO_2 nanotube arrays

ABSTRACT

TiO_2 nanotube arrays can be synthesized by several experimental procedures. Here we construct the first theoretical model of the array. Based on the density functional theory calculations, the formation energy of the TiO_2 nanotube array is nearly the same as that of rutile TiO_2 (1 1 0) surface. Moreover the electronic properties of TiO_2 nanotube arrays have been analyzed. The thermodynamic properties of H_2O splitting on the TiO_2 nanotube and nanotube arrays have been discussed using the density functional theory calculations and Gibbs free energy diagrams. The overpotential of H_2O splitting is 0.51 and 1.0 eV on the outside and inside of nanotube and 1.13 eV on the inside TiO_2 nanotube of an array.

1. Introduction

Photoelectrochemical water splitting utilizing solar energy for the electrolysis of water [1–4] is a vital step in the hydrogen economy. The photoelectrochemical cells consist of the semiconductor photoanode and a metal cathode, at which oxygen and hydrogen is evolved, respectively. The photoanode materials are the most important factor in determining the efficiency of water splitting since the anode reaction exhibits slower kinetics than the cathode reaction and requires more energy.

Ideal photoanode materials should have excellent stability, suitable band gap (at least larger than 1.7 eV) that matches the H_2O oxidation and reduction potentials. At present, the most used photoanode materials are the metal oxides, for example RuO_2 [5,6], IrO_2 [7], TiO_2 [8–10], ZnO [11,12] etc. Among them, TiO_2 is the most well studied due to its' excellent optic, electrochemical, and mechanical properties [8–10,13–15]. However, TiO_2 is only responsive to UV light due to its large band gap (about 3.2 eV), which cannot utilize the visible light (about 45% of solar energy). In order to narrow the band gap and modify the energy levels, various methods have been attempted, including noble metal loading [16], ion doping [17,18], sensitization and metal ion-implantation. So far, these modifications have not met the requirements for effective utilization of visible light of solar energy.

Recently, TiO_2 nanotube arrays have attracted much attention due to their large internal surface area and the highly order geometrical structures [19–26]. Especially, they possess outstanding charge transport and carrier lifetime properties since they have electron percolation pathways for vectorial charge transfer between interfaces. These excellent properties make them suitable for a series of applications in sensors [27,28], dye sensitized solar cells [29–34], hydrogen generation from water photoelectrolysis [35–37], photoreduction of CO_2 under outdoor sunlight [38]. By using the highly ordered titania nanotube arrays, Mor et al. reported the highest hydrogen generation rate for a titania-based photoelectrochemical cell [19]. The p-type Cu–Ti–O nanotube arrays have a complete visible spectrum photoresponse [20], which can enhance oxygen and hydrogen evolution. The carbon-doped TiO_2 nanotube arrays show efficient water splitting under visible-light illumination [21]. By introducing highly dispersed metal (Ir and Co) particles in the texture of TiO_2 nanotube arrays, hydrogen and oxygen can be produced by the water splitting under the visible light irradiation [25]. Although TiO_2 nanotube arrays show better water splitting properties than TiO_2 nanoparticles, the enhanced mechanism at the electronic level is still unknown.

Theoretically, compared with many experimental studies on the preparation and application of TiO_2 nanotubes arrays, few studies have been conducted on the structures and properties of the TiO_2 nanotube. The formation mechanism and various electronic properties of titanate nanotubes [39–41], TiO_2 nanotubes formed from the anatase (1 0 1) surface [42,43] and built by a reconstructed (0 0 1) bilayer of rutile [44] or hexagonal ABC PtO_2 structure [45] have been investigated. Recently, we constructed TiO_2 nanotubes from single trilayer rutile TiO_2 (1 1 0) thin sheets [46], which is similar to the formation of carbon nanotubes from a graphene sheet.

* Corresponding author at: Institute of Industrial Catalysis, College of Chemical Engineering and Materials Science, 18, Chaowang Road, Hangzhou 310032, China. Tel.: +86 571 88871037, fax: +86 571 88871037.
E-mail address: jgw@zjut.edu.cn (J.-g. Wang).

0920-5861/$ – see front matter © 2010 Elsevier B.V. All rights reserved.
doi:10.1016/j.cattod.2010.11.086

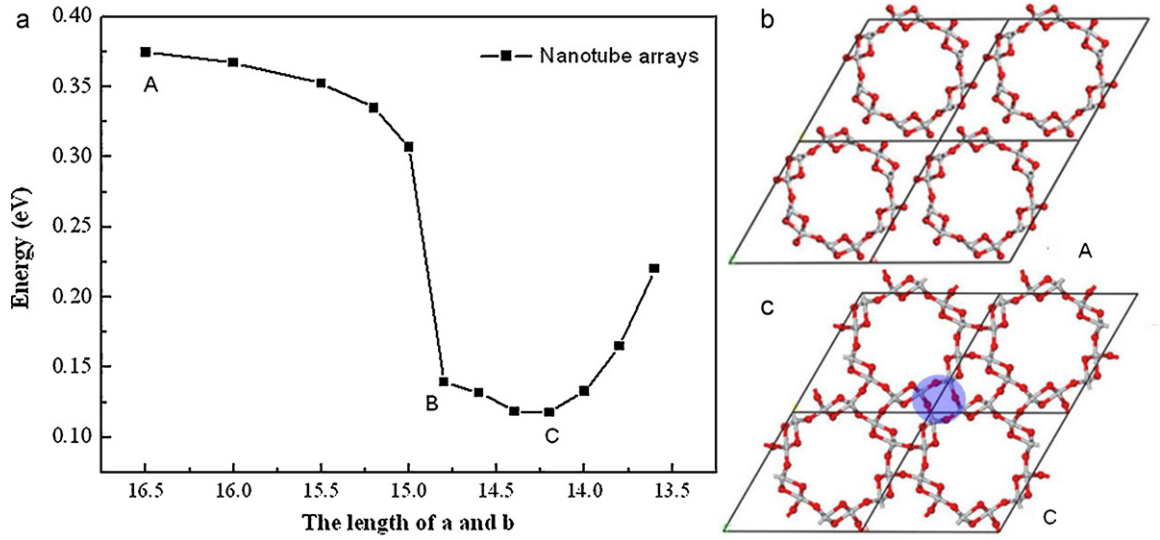

Fig. 1. (a) The formation energies of the TiO_2 nanotube array with different unit cell parameters ($b = a$). (A) $a = 16.5$ Å, (B) $a = 14.8$ Å, (C) $a = 14.2$ Å. The optimized structures of TiO_2 nanotube arrays are shown in (b) A, (c) C.

However, to the best of our knowledge, no theoretical studies on TiO_2 nanotube arrays have been reported.

In this study, models of TiO_2 nanotube arrays have been proposed and the geometric and electronic properties of TiO_2 nanotube arrays have been investigated in detail. Based on density functional theory (DFT) calculations and Gibbs free energy diagrams, the thermodynamic properties of H_2O splitting on the TiO_2 nanotube and nanotube array have been discussed. The overpotential of H_2O splitting is 0.51 and 1.0 eV on the outside and inside of the nanotube and 1.13 eV on inside TiO_2 nanotube of an array.

2. Methods

2.1. DFT calculations

The computations have been carried out using the plane-wave approach, together with the Perdew–Burke–Ernzerhof (PBE) [47] exchange-correlation functional, and ultrasoft pseudopotentials [48] with PWSCF code implemented in Quantum-Espresso [49]. The plane-wave basis set cutoffs for the smooth part of the electron wave functions and augment electron density is 25 and 200 Ry, respectively. The TiO_2 nanotube arrays are formed by the most stable TiO_2 (6, 6) nanotubes built from the reconstructed single tri-layer rutile (1 1 0) sheet [46]. The periodic boundary condition was used with a supercell of 14.2 Å × 14.2 Å × 2.97 Å. The suitable Monkhorst–Pack k-point sampling is $2 \times 2 \times 8$ after testing different k-point grids. All of the atoms were fully relaxed until each component of the residual force on each atom was smaller than 0.03 eV/Å.

For H_2O splitting, the geometry optimization and vibration frequencies calculations have been carried out by using the DMol^3 code [50,51] with double-numerical polarized (DNP) basis sets. Our calculations were performed with the PW91 and the k-point sampling was performed in a $2 \times 2 \times 4$ Monkhorst–Pack mesh. The unit cell of TiO_2 nanotube arrays used in the H_2O splitting is 14.2 Å × 14.2 Å × 8.91 Å, which consists of 36 Ti and 72 O atoms.

2.2. Gibbs free energy diagrams

The water splitting reaction separates into the oxidation and reduction processes.

Oxidation:

$$2H_2O \rightarrow O_2 + 4H^+ + 4e^- \quad (1)$$

Reduction:

$$2H^+ + 2e^- \rightarrow H_2 \quad (2)$$

Overall:

$$2H_2O \rightarrow O_2 + 2H_2 \quad (3)$$

We assume that one-electron transfer elementary steps of the oxidation reaction are:

$$A : 2H_2O + * \rightarrow H_2O + HO* + H^+ + e^-$$

$$B : H_2O + HO* + H^+ + e^- \rightarrow H_2O + O* + 2(H^+ + e^-)$$

$$C : H_2O + O* + 2(H^+ + e^-) \rightarrow OOH* + 3(H^+ + e^-)$$

$$C : H_2O + O* + 2(H^+ + e^-) \rightarrow OOH* + 3(H^+ + e^-)$$

We used the same scheme to obtain the free-energy differences between the intermediates proposed by Norskov et al. [52–55] which has been widely used to investigate the thermochemistry of H_2O splitting, O_2 reduction reactions on metal and metal oxide surfaces. In these methods, the Gibbs free energy for each elementary step is calculated from:

$$\Delta G = \Delta E + \Delta ZPE - T\Delta S + \Delta G_{pH} + \Delta G_U \quad (4)$$

where ΔE is the reaction energy, obtained from DFT calculations; the differences in zero-point energies, ΔZPE, are calculated using DFT vibrational frequencies analysis; $T\Delta S$, change in entropy using standard tables for gas-phase molecules; ΔG_{pH} and ΔG_U, the free energy contributions due to the variations of H^+ concentration and electrode potential. In this study, we did not consider the influence of pH on the Gibbs free energies by fixing the pH (pH = 0). The chemical potential for $H^+ + e^-$ is related to $1/2H_2$ in the gas phase since the reference potential is the standard hydrogen electrode (NHE).

3. Results and discussion

3.1. Geometric structures of nanotube arrays

We first build the models of TiO_2 nanotube arrays since no theoretical models have been reported. It is well known that carbon nanotube arrays are formed by Van der Waals' forces between carbon nanotubes. Both carbon nanotube and carbon nanotube arrays are experimentally available. It should be mentioned that the structures of TiO_2 nanotube arrays may be different from those of carbon nanotube arrays since these TiO_2 nanotubes can be connected by the strong chemical bonds.

The stable single-walled TiO_2 (6, 6) nanotubes identified from our previous study [46] are placed in the hexagonal unit cell ($a = b = 16.5$ Å, $c = 2.97$ Å, $\alpha = 90°$, $\beta = 90°$, $\gamma = 60°$). By changing the lattice parameter (a, b), the distances between TiO_2 nanotube are reduced until the nanotube arrays formed. Of course, during the optimization process, the positions of TiO_2 need to adjust in order to get the most stable TiO_2 nanotube arrays. The formation energies per TiO_2 subunit at different lengths of a and b ($a = b$) are shown in Fig. 1 (a), in which the formation energies monotonically decrease from 0.37 to 0.30 eV when a is reduced from 16.5 to 15.0 Å (structure A shown in Fig. 1 (b)). When a (b) is 14.2 Å, the most stable TiO_2 nanotube arrays (structure C) are formed (as shown in Fig. 1 (c)). It can be seen that these arrangements of TiO_2 nanotubes are also consistent with the hexagonal close-packed structures, which is very similar to the experimental observed structures [56–59]. The distances between Ti and oxygen (in the blue part of the neighboring TiO_2 nanotubes) are 1.84 and 2.08 Å in the structure C. It should be mentioned that TiO_2 (6, 6) used in this study are composed of 12 TiO_2 subunits. All of the unsaturated oxygen and titanium atoms in the TiO_2 nanotubes [46] are bonded with the neighboring TiO_2 nanotubes of the arrays. Therefore, the coordination numbers of oxygen and titanium are three and six, which are the same as those in the bulk TiO_2. Of course, for larger diameters of TiO_2 nanotube arrays, some of the oxygen and titanium atoms will still have unsaturated coordination.

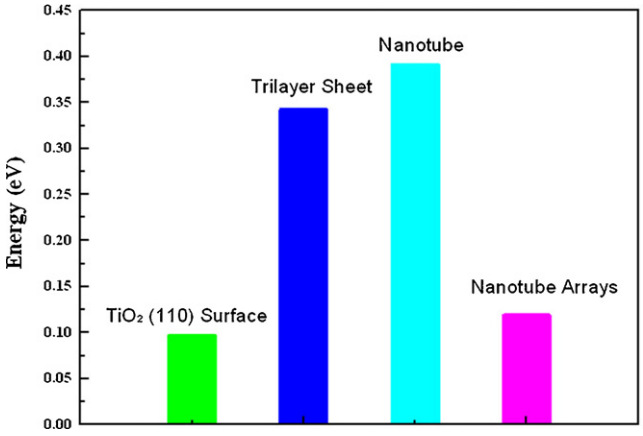

Fig. 2. The formation energies of rutile TiO_2 (1 1 0) surface, single tri-layer sheet, TiO_2 nanotube and TiO_2 nanotube arrays.

Furthermore, we compared the formation energies of the arrays with other TiO_2 structures in Fig. 2. It can be seen that the formation energy of TiO_2 nanotube arrays is 0.12 eV, which is very close to the most stable rutile TiO_2 (1 1 0) surface and much more stable than the tri-layer sheet and single-walled nanotubes [46].

3.2. Electronic structures of TiO_2 nanotube arrays

The calculated band structures, projected density of states (PDOS) of Ti and oxygen, the highest occupied and lowest unoccupied molecular orbitals of the investigated TiO_2 nanotube arrays are shown in Fig. 3. The band gaps of TiO_2 nanotube arrays and single-walled TiO_2 nanotube are 3.02 and 3.35 eV [46], which corresponds to direct and indirect semiconductor, respectively, according to the

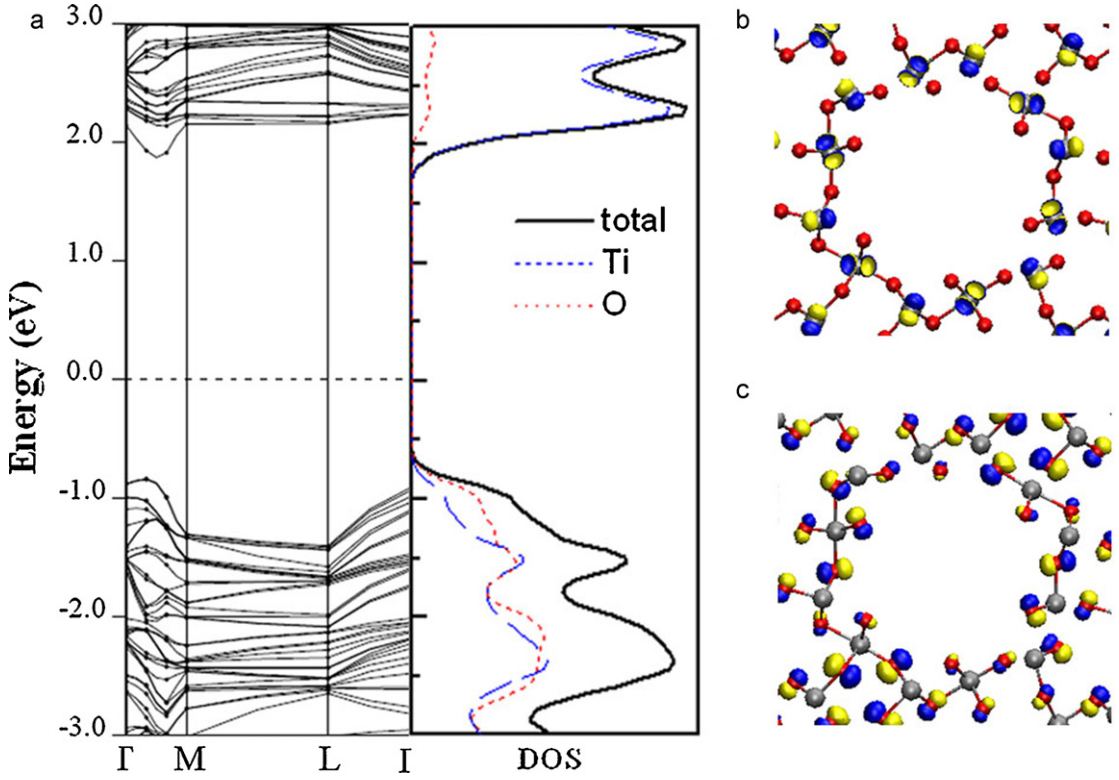

Fig. 3. (a) The calculated band structures, density of states (DOS) and projected DOS of the TiO_2 nanotube array. (b) The lowest unoccupied molecular orbitals. (c) The highest occupied molecular orbitals of TiO_2 nanotube array.

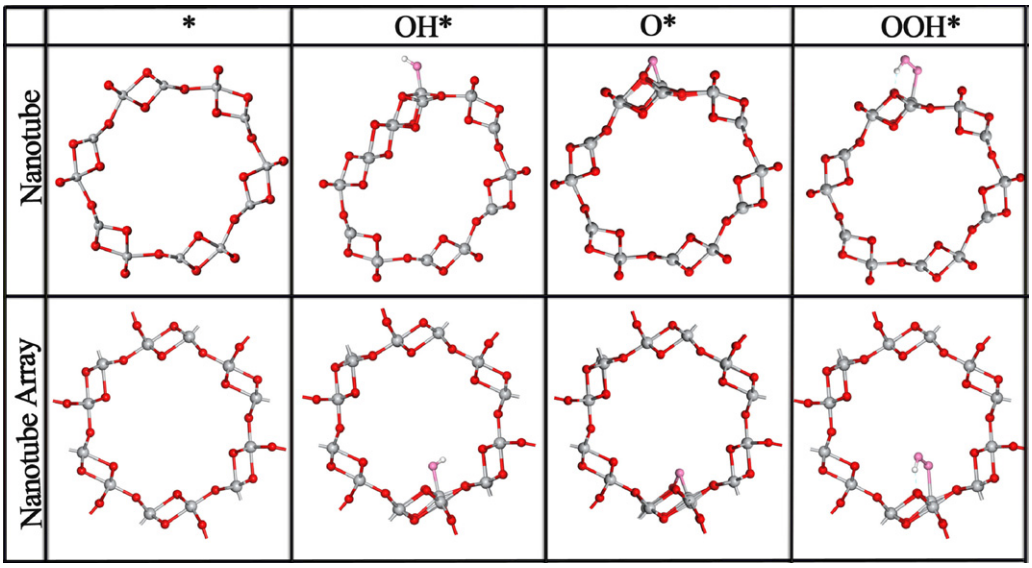

Fig. 4. The optimized intermediate structures for the oxygen evolution from H_2O splitting on (a) the outside wall of TiO_2 nanotube and (b) inside TiO_2 nanotube of an array.

band structure analysis. From our study, we found that the calculated band gap of TiO_2 nanotube or nanotube arrays is bigger (about 1.0 eV) than that of bulk TiO_2. Several recent theoretical studies [60–62] on other metal oxide nanotubes reported similar observations. Moreover, the projected local density of states (PDOS) is also plotted in Fig. 3. From the PDOS spectra we can see that the low valence and high conduction bands are mainly from oxygen and Ti. Indeed, the HOMO and LUMO orbitals of the nanotube array are contributed from oxygen and Ti which is very similar to the single nanotube.

3.3. H_2O splitting on TiO_2 nanotube and nanotube arrays

In this section, the water oxidation reaction on the TiO_2 nanotube [46] and nanotube arrays are discussed and the corresponding free energy diagrams under different applied potential U and fixed pH (pH = 0 in this study) are presented. The reaction intermediates of H_2O splitting on TiO_2 nanotube and nanotube array are shown in Fig. 4. Due to the similar configurations of these reaction intermediates on the inside of TiO_2 nanotube and nanotube arrays, only the geometries of the TiO_2 nanotube arrays are shown. The hydroxyl (OH*) via the dissociation of first H_2O adsorbs on the top site of Ti (step A). Next, the adsorbed oxygen (O*) via the dehydrogenation of OH is on the bridge site of Ti–O (step B). Furthermore, the OOH* is formed by the oxygen (O*) and the second H_2O (step C). Finally, O_2 is released from the nanotube and nanotube array (step D). From Fig. 4, it can be seen the adsorbed species can induce structure deformation of TiO_2 nanotube. However, the structure of TiO_2 nanotube arrays is not significantly affected.

According to the formula (4), the Gibbs free energies of the elementary steps of H_2O splitting on the outside and the inside of a TiO_2 nanotube and inside the nanotube of an array are shown in Figs. 5–7. For each diagram, three different potentials have been given and plotted: the open cell potential 0 V, the equilibrium potential 1.23 V, and the lowest potential. Under the lowest potential, the free energy changes of all of the elementary steps are negative or zero, which are dependent on the specific nanomaterials. The difference between the lowest potential and the equilibrium (1.23 V) is termed as the theoretical overpotential, which is an important indicator to evaluate the electrochemical catalytic activity of materials. From Figs. 5–7, we found that the lowest potential of H_2O splitting on the outside and inside of TiO_2 nanotube is 1.74 and 2.23 eV, respectively, and that of inside nan-

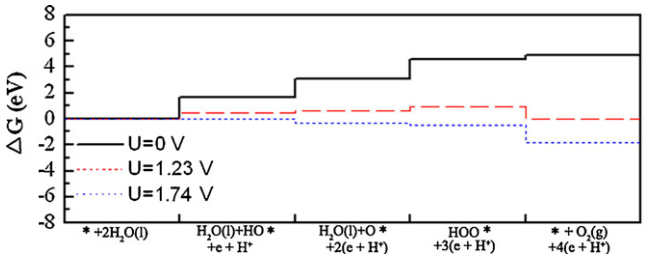

Fig. 5. Calculated free energies of intermediates following the oxygen evolution from H_2O splitting on the outside wall of a TiO_2 nanotube at three potentials (relative to the standard hydrogen electrode); zero potential (U = 0 V), the equilibrium potential (U = 1.23 V) and the lowest potential at which all steps are downhill in free energy (U = 1.68 V).

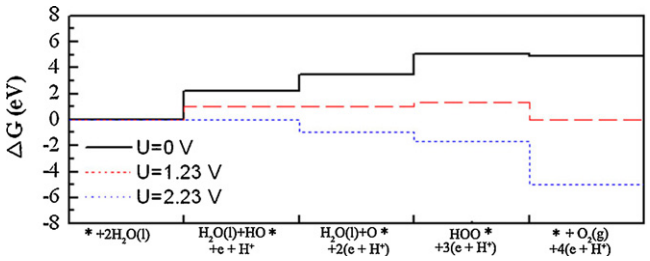

Fig. 6. Calculated free energies of intermediates following the oxygen evolution from H_2O splitting on the inside wall of a TiO_2 nanotube at three potentials (relative to the standard hydrogen electrode); zero potential (U = 0 V), the equilibrium potential (U = 1.23 V) and the lowest potential at which all steps are downhill in free energy (U = 2.23 V).

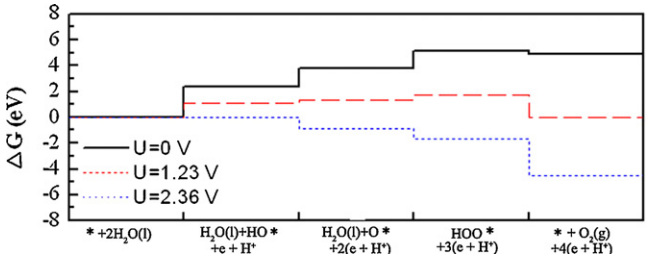

Fig. 7. Calculated free energies of intermediates following the oxygen evolution from H_2O splitting on inside TiO_2 nanotube of an array at three potentials (relative to the standard hydrogen electrode); zero potential (U = 0 V), the equilibrium potential (U = 1.23 V) and the lowest potential at which all steps are downhill in free energy (U = 2.36 V).

otube of the array is 2.36 eV, which all correspond to the first step on the three kinds of nanostructures. Based on the thermodynamic point of view from the Gibbs free analysis, the rate-limiting step is to obtain the OH from the dissociation of the first H_2O on both TiO_2 nanotube and nanotube arrays. The overpotential of H_2O splitting on the outside and inside of TiO_2 nanotube is 0.51 and 1.0 eV, respectively and that of inside TiO_2 nanotube of the array is 1.13 eV. We found that the overpotential of H_2O splitting on the outside of TiO_2 nanotube is nearly the same as that of RuO_2 (0.37 eV) [52], which is one of the best known inorganic catalysts for H_2O splitting or O_2 evolution. While for H_2O splitting on the inside of either TiO_2 nanotube and TiO_2 nanotube arrays, the overpotential is much larger than that on the outside of TiO_2 nanotube, which is even larger than that on TiO_2 (1 1 0) surface [53–55]. The large overpotential of H_2O splitting on the inside of TiO_2 nanotube or nanotube arrays are probably caused by the small diameter nanotube used in this study. In the future, we will investigate the effect of tube diameter as well as defects and dopants on H_2O splitting in the TiO_2 nanotube arrays.

4. Conclusions

We constructed the first models of TiO_2 nanotube arrays. The formation energy of TiO_2 nanotube arrays is nearly the same as rutile TiO_2 (1 1 0) surface based on the density functional theory calculations. The thermodynamic properties of H_2O splitting on the TiO_2 nanotube and nanotube array have been discussed based on the Gibbs free energy diagrams. The overpotential of H_2O splitting is 0.51 and 1.0 eV on the outside and inside of nanotube and 1.13 eV on the inside of nanotube arrays. Based on the thermodynamic point of view from the Gibbs free analysis, the rate-limiting step is to obtain the OH from the dissociation of the first H_2O on both TiO_2 nanotube and nanotube arrays.

Acknowledgements

This work was supported by the National Natural Science Foundation of China (No. 20906081), the "Qianjiang Scholars" program of Zhejiang Province, and the Key Projects of Science and Technology Research of the Ministry of Education of China (No. 209055).

References

[1] Z.G. Zou, J.H. Ye, K. Sayama, H. Arakawa, Nature 414 (2001) 625–627.
[2] K. Sivula, R. Zboril, F. Le Formal, R. Robert, A. Weidenkaff, J. Tucek, J. Frydrych, M. Gratzel, Journal of the American Chemical Society 132 (2010) 7436–7444.
[3] F. Le Formal, M. Gratzel, K. Sivula, Advanced Functional Materials 20 (2010) 1099–1107.
[4] K. Sivula, F. Le Formal, M. Gratzel, Chemistry of Materials 21 (2009) 2862–2867.
[5] N. Arai, N. Saito, H. Nishiyama, K. Domen, H. Kobayashi, K. Sato, Y. Inoue, Catalysis Today 129 (2007) 407–413.
[6] H. Kadowaki, N. Saito, H. Nishiyama, H. Kobayashi, Y. Shimodaira, Y. Inoue, Journal of Physical Chemistry C 111 (2007) 439–444.
[7] W.J. Youngblood, S.H.A. Lee, K. Maeda, T.E. Mallouk, Accounts of Chemical Research 42 (2009) 1966–1973.
[8] H. Liu, J. Gao, M.Q. Xue, N. Zhu, M.N. Zhang, T.B. Cao, Langmuir 25 (2009) 12006–12010.
[9] J.W. Tang, J.R. Durrant, D.R. Klug, Journal of the American Chemical Society 130 (2008) 13885–13891.
[10] A.F. Feil, P. Migowski, F.R. Scheffer, M.D. Pierozan, R.R. Corsetti, M. Rodrigues, R.P. Pezzi, G. Machado, L. Amaral, S.R. Teixeira, D.E. Weibel, J. Dupont, Journal of the Brazilian Chemical Society 21 (2010) 1359–1365.
[11] H.M. Chen, C.K. Chen, Y.C. Chang, C.W. Tsai, R.S. Liu, S.F. Hu, W.S. Chang, K.H. Chen, Angewandte Chemie International Edition 49 (2010) 5966–5969.
[12] S. Shet, K.S. Ahn, T. Deutsch, H.L. Wang, R. Nuggehalli, Y.F. Yan, J. Turner, M. Al-Jassim, Journal of Power Sources 195 (2010) 5801–5805.
[13] J.G. Wang, B. Hammer, Physical Review Letters 97 (2006).
[14] D. Matthey, J.G. Wang, S. Wendt, J. Matthiesen, R. Schaub, E. Laegsgaard, B. Hammer, F. Besenbacher, Science 315 (2007) 1692–1696.
[15] S.C. Li, J.G. Wang, P. Jacobson, X.Q. Gong, A. Selloni, U. Diebold, Journal of the American Chemical Society 131 (2009) 980–984.
[16] D. Yang, S.W. Lee, Surface Review Letters 17 (2010) 21–26.
[17] T. Ando, T. Wakamatsu, K. Masuda, N. Yoshida, K. Suzuki, S. Masutani, I. Katayama, H. Uchida, H. Hirose, A. Kamimoto, Applied Surface Science 255 (2009) 9688–9690.
[18] H. Zhou, X.F. Li, T.X. Fan, F.E. Osterloh, J. Ding, E.M. Sabio, D. Zhang, Q.X. Guo, Advanced Materials 22 (2010) 951.
[19] G.K. Mor, K. Shankar, M. Paulose, O.K. Varghese, C.A. Grimes, Nano Letters 5 (2005) 191–195.
[20] G.K. Mor, O.K. Varghese, R.H.T. Wilke, S. Sharma, K. Shankar, T.J. Latempa, K.S. Choi, C.A. Grimes, Nano Letters 8 (2008) 1906–1911.
[21] J.H. Park, S. Kim, A.J. Bard, Nano Letters 6 (2006) 24–28.
[22] C.J. Lin, Y.T. Lu, C.H. Hsieh, S.H. Chien, Applied Physics Letters 94 (2009).
[23] J. Jitputti, Y. Suzuki, S. Yoshikawa, Catalysis Communications 9 (2008) 1265–1271.
[24] M.A. Khan, M.S. Akhtar, S.I. Woo, O.B. Yang, Catalysis Communications 10 (2008) 1–5.
[25] M.A. Khan, O.B. Yang, Catalysis Today 146 (2009) 177–182.
[26] J.J. Gong, Y.K. Lai, C.J. Lin, Electrochimica Acta 55 (2010) 4776–4782.
[27] Q. Zheng, B.X. Zhou, J. Bai, L.H. Li, Z.J. Jin, J.L. Zhang, J.H. Li, Y.B. Liu, W.M. Cai, X.Y. Zhu, Advanced Materials 20 (2008) 1044.
[28] A.S. Zuruzi, A. Kolmakov, N.C. MacDonald, M. Moskovits, Applied Physics Letters 88 (2006).
[29] D. Kuang, J. Brillet, P. Chen, M. Takata, S. Uchida, H. Miura, K. Sumioka, S.M. Zakeeruddin, M. Gratzel, ACS Nano 2 (2008) 1113–1116.
[30] D.A. Wang, Y. Liu, C.W. Wang, F. Zhou, W.M. Liu, ACS Nano 3 (2009) 1249–1257.
[31] T.S. Kang, A.P. Smith, B.E. Taylor, M.F. Durstock, Nano Letters 9 (2009) 601–606.
[32] G.K. Mor, K. Shankar, M. Paulose, O.K. Varghese, C.A. Grimes, Nano Letters 6 (2006) 215–218.
[33] K. Shankar, J. Bandara, M. Paulose, H. Wietasch, O.K. Varghese, G.K. Mor, T.J. LaTempa, M. Thelakkat, C.A. Grimes, Nano Letters 8 (2008) 1654–1659.
[34] K. Zhu, N.R. Neale, A. Miedaner, A.J. Frank, Nano Letters 7 (2007) 69–74.
[35] G.K. Mor, H.E. Prakasam, O.K. Varghese, K. Shankar, C.A. Grimes, Nano Letters 7 (2007) 2356–2364.
[36] K. Shankar, G.K. Mor, H.E. Prakasam, S. Yoriya, M. Paulose, O.K. Varghese, C.A. Grimes, Nanotechnology 18 (2007) 065707.
[37] N.K. Allam, K. Shankar, C.A. Grimes, Journal of Materials Chemistry 18 (2008) 2341–2348.
[38] O.K. Varghese, M. Paulose, T.J. LaTempa, C.A. Grimes, Nano Letters 9 (2009) 731–737.
[39] A.N. Enyashin, A.L. Ivanovskii, Journal of Physical Chemistry C 113 (2009) 20837–20840.
[40] X.G. Xu, X. Ding, Q. Chen, L.M. Peng, Physical Review B (2006) 73.
[41] M. Casarin, A. Vittadini, A. Selloni, ACS Nano 3 (2009) 317–324.
[42] A.V. Bandura, R.A. Evarestov, Surface Science 603 (2009) L117–L120.
[43] P. Gualco, T.P. Lin, M. Sircoglou, M. Mercy, S. Ladeira, G. Bouhadir, L.M. Perez, A. Amgoune, L. Maron, F.P. Gabbai, D. Bourissou, Angewandte Chemie International Edition 48 (2009) 9892–9895.
[44] T. He, M.W. Zhao, X.J. Zhang, H.Y. Zhang, Z.H. Wang, Z.X. Xi, X.D. Liu, S.S. Yan, Y.Y. Xia, L.M. Mei, Journal of Physical Chemistry C 113 (2009) 13610–13615.
[45] D.J. Mowbray, J.I. Martinez, J.M.G. Lastra, K.S. Thygesen, K.W. Jacobsen, Journal of Physical Chemistry C 113 (2009) 12301–12308.
[46] Q.Q. Meng, J.G. Wang, Q. Xie, X.N. Li, Journal of Physical Chemistry C 114 (2010) 9251–9256.
[47] J.P. Perdew, K. Burke, M. Ernzerhof, Physical Review B 77 (1996) 3865.
[48] D. Vanderbilt, Physical Review B 41 (1990) 7892.
[49] P. Giannozzi, S. Baroni, N. Bonini, M. Calandra, R. Car, C. Cavazzoni, D. Ceresoli, G.L. Chiarotti, M. Cococcioni, I. Dabo, A. Dal Corso, S. Fabris, G. Fratesi, S. de Gironcoli, R. Gebauer, U. Gerstmann, C. Gougoussis, M.L.A. Kokalj, L. Martin-Samos, N. Marzari, F. Mauri, R. Mazzarello, S. Paolini, A. Pasquarello, L. Paulatto, C. Sbraccia, S. Scandolo, G. Sclauzero, A.P. Seitsonen, A. Smogunov, P. Umari, R.M. Wentzcovitch, Journal of Physics: Condensed Matter 21 (2009) 395502.
[50] B. Delley, Journal of Chemical Physics 92 (1990) 508–517.
[51] B. Delley, Journal of Chemical Physics 113 (2000) 7756–7764.
[52] J. Rossmeisl, K. Dimitrievski, P. Siegbahn, J.K. Norskov, Journal of Physical Chemistry C 111 (2007) 18821–18823.
[53] J. Rossmeisl, A. Logadottir, J.K. Norskov, Chemical Physics 319 (2005) 178–184.
[54] J. Rossmeisl, Z.W. Qu, H. Zhu, G.J. Kroes, J.K. Norskov, Journal of Electroanalytical Chemistry 607 (2007) 83–89.
[55] A. Valdes, Z.W. Qu, G.J. Kroes, J. Rossmeisl, J.K. Norskov, Journal of Physical Chemistry C 112 (2008) 9872–9879.
[56] G.K. Mor, O.K. Varghese, M. Paulose, K. Shankar, C.A. Grimes, Solar Energy Materials and Solar Cells 90 (2006) 2011–2075.
[57] K. Shankar, J.I. Basham, N.K. Allam, O.K. Varghese, G.K. Mor, X.J. Feng, M. Paulose, J.A. Seabold, K.S. Choi, C.A. Grimes, Journal of Physical Chemistry C 113 (2009) 6327–6359.
[58] M. Paulose, K. Shankar, O.K. Varghese, G.K. Mor, B. Hardin, C.A. Grimes, Nanotechnology 17 (2006) 1446–1448.
[59] K. Shankar, G.K. Mor, H.E. Prakasam, S. Yoriya, M. Paulose, O.K. Varghese, C.A. Grimes, Nanotechnology (2007) 18.
[60] A.M. Ferrari, D. Szieberth, C.M. Zicovich-Wilson, R. Demichelis, Journal of Physical Chemistry Letters 1 (2010) 2854–2857.
[61] W. An, X.J. Wu, X.C. Zeng, Journal of Physical Chemistry C 112 (2008) 5747–5755.
[62] D.Q. Fang, A.L. Rosa, R.Q. Zhang, T. Frauenheim, Journal of Physical Chemistry C 114 (2010) 5760–5766.